



Cite this: *Phys. Chem. Chem. Phys.*,
2017, 19, 21401

Recognition of chiral zwitterionic interactions at nanoscale interfaces by chiropasmonic nanosensors†

Wenjing Zhao,^a Rong-Yao Wang,^b Hong Wei,^b Jingliang Li,^c Yinglu Ji,^d
Xinxin Jiang,^a Xiaochun Wu^b and Xiangdong Zhang^b

The ability to detect chiral molecules renders plasmonic nanosensors as promising tools for the study of chirality phenomena in living systems. Using gold nanorod based plasmonic nanosensors, we investigated here typically chiral zwitterionic electrostatic (Zw-Es) and hydrogen-bonding (Hb) interactions occurring via amine and carboxylic groups at nanoscale interfaces in aqueous solutions. Our results reveal that the plasmonic circular dichroism responses of the nanosensors can have both conformational sensitivity and chiral selectivity to the interfacial molecular interactions. Such a dual function of the plasmonic nanosensors enables a new chiroptical way to differentiate between chiral Zw-Es and Hb interactions, to monitor the transformation between these two interaction forces, and particularly to recognize homochiral Zw-Es interactions in solution. Together with the surface enhanced Raman scattering (SERS) technique, this plasmonic CD based biosensing could have important values for the insightful understanding of chirality-dependent molecular recognition in biological and pharmaceutical systems.

Received 7th May 2017,
Accepted 30th May 2017

DOI: 10.1039/c7cp03004e

rsc.li/pccp

Introduction

Chirality-controlled molecular recognition plays a pivotal role in the activities of biological systems. A prominent example is the recognition of the enantiomeric pair (*R* and *S*) of a chiral drug, which can have significantly different potency and toxicity in our living systems. At the molecular level, such chirality recognition occurs normally at the nanoscale interfaces of biomolecules,^{1–3} and the host–guest homochiral or heterochiral recognitions may involve different intermolecular interactions, *e.g.* different interacting sites and/or different relative orientations/distances of the interacting groups.^{4,5} The detection and characterization of those interfacial chiral interactions are essential for understanding the underlying physical mechanisms. To this end, powerful tools that possess not only sensitivity to the interfacial molecular interactions but also selectivity towards the chirality information are highly desired.

Traditional chiroptical techniques, such as electronic CD,⁶ vibrational CD,⁷ and Raman optical activity,⁸ are common tools

for detecting and characterizing the chirality of biomolecular interactions in solution phases. Unfortunately, the inherently weak optical activities of biomolecules mean these chiroptical measurements suffer from poor sensitivity to the chiral interactions at the nanoscale interfaces. In comparison, modern biosensing techniques,^{9,10} especially those based on the unique optical properties of semiconductor and metallic nanoparticles, can provide ultrasensitive detection for such interfacial biomolecular interactions. Excellent examples include Au, Ag, and CdS nanoparticle based biosensors that are able to distinguish the host–guest homochiral and heterochiral interactions by absorption,¹¹ fluorescence,¹² and Raman scattering^{13,14} spectroscopy. These techniques, however, are all based on the measurement of the nonchiral properties, thus lacking selectivity to the chiral information of biomolecular interactions.

Very recently, advancement in chiropasmonic nanosensors^{15,16} has offered an opportunity to overcome the aforementioned detection limitations. Of particular interest is Ag and/or Au nanoparticle based CD sensing,^{17–19} which detects weak molecular CD signals (normally in the UV region) by strong chiroptical responses to the surface plasmon resonance (SPR) absorptions in the Vis/NIR region. In a number of experiments, the plasmonic CD responses of these nanosensors were used to detect DNA,^{18,20–22} amino acids,^{17,23–26} and peptides,²⁷ demonstrating a much higher sensitivity than that by conventional electronic CD measurements. As a new chiroptical technique, plasmonic CD spectroscopy is presumed to possess both

^a The Key Laboratory of Cluster Science of Ministry of Education, School of Physics, Beijing Institute of Technology, 100081 Beijing, China. E-mail: wangry@bit.edu.cn

^b Institute of Physics, Chinese Academy of Sciences, 100190 Beijing, China

^c Institute for Frontier Materials, Deakin University, 3216 Victoria, Australia

^d CAS Key Laboratory of Standardization and Measurement for Nanotechnology, CAS Center for Excellence in Nanoscience, National Center for Nanoscience and Technology, 100190 Beijing, China

† Electronic supplementary information (ESI) available. See DOI: 10.1039/c7cp03004e

conformational sensitivity and chiral selectivity to the biomolecular adsorptions and interactions at interfaces, since the electromagnetically induced CD effects would depend strongly on the chirality signatures and configurations (*i.e.* orientations and conformations) of the biomolecules.^{28–30} However, so far very few experimental studies have addressed this dual function of plasmonic CD nanosensors.¹⁸

In this work, we explore the use of plasmonic CD nanosensors for the *in situ* detection of different interfacial chiral interactions of biomolecules in the solution phase. Gold nanorods (GNRs) functionalized with cysteine (Cys) molecules are used as a model system. In the combination of plasmonic CD with SERS spectroscopy, we investigate Cys mediated interfacial chiral Zw-Es and Hb interactions in neutral or acidic solutions. Our study reveals here the new function of plasmonic CD based chiroptical sensing to recognize different chiral interactions in terms of their conformational sensitivity and chiral selectivity to the molecular interactions at interfaces.

Experimental section

Discrete GNRs capped with positively charged stabilizers (*i.e.* cetyltrimethylammonium bromide, CTAB) were prepared by the seed-mediated method.²⁴ We used here GNRs with an average size of $\sim 41 \times 17$ nm. Using the method described in ref. 25, we prepared discrete GNRs functionalized with chiral patches of an enantiopure (*L*- or *D*-) and racemic mixture (*rac*-) of Cys molecules on their end surfaces (see ESI† for the Experimental details). These chiral patched nanorods are hereafter referred to as *L*-, *D*-, and *rac*-GNRs. As demonstrated in previous studies,^{31–34} the Cys molecules adsorb at the end surfaces of the GNRs *via* strong Au–S bonds (upper panel, Fig. 1), and Cys mediated interparticle interactions can drive the end-to-end (EE) assembly of GNRs. Specifically, Cys mediated Zw-Es interactions^{31,35} (lower left panel, Fig. 1) can be the major driving force for the EE assembly of GNRs in a neutral solution; while in an acidic solution the EE assembly of GNRs can be promoted by Hb interactions *via* protonated and unprotonated Cys molecules³³ (lower right panel, Fig. 1). Apparently, chiral Zw-Es and Hb interactions involve different “contact-points”³⁶ *via* three “fingers” (H, NH₂, and COOH) bonded with the chiral C center of the Cys molecules. Our experiments below will investigate how the distinct molecular conformations and chiral natures involved in these two kinds of interactions affect the chiroplasmonic properties of the GNR nanosensors during the assembly processes.

Besides the Cys mediated chiral Zw-Es/Hb forces, other interparticle forces also play an important role in the EE assembly of GNRs in solution. Of particular importance is the electrostatic (repulsive) force mediated by the CTAB stabilizer (at the side-surfaces of the GNRs). Compared to the short-ranged Zw-Es and/or Hb (attractive) forces mediated by the Cys patches, the CTAB mediated repulsive force is long-ranged and depends on the molecular density and electrostatic double layers surrounding the nanoparticles.^{37,38} The balance between the repulsive and attractive forces is a key factor affecting the assembly kinetics

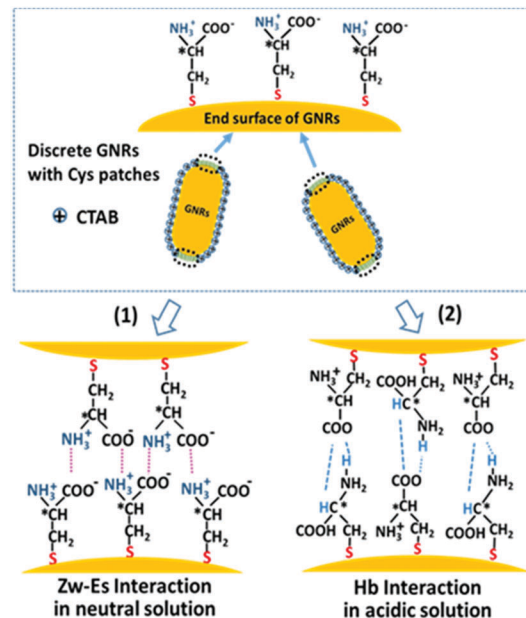


Fig. 1 Schematic illustration of GNR based chiroplasmonic nanosensors for detecting the interfacial chiral Zw-Es and Hb interactions during the self-assembly processes. (Upper panel) CTAB stabilized GNRs functionalized with chiral Cys patches at the end-surfaces in the neutral solution phase. (Lower panels) Two different Cys mediated chiral interactions in an end-to-end assembly of GNRs: (1) Zw-Es interaction in neutral solution; (2) Hb interaction in acidic solution.

and consequently the structure and chiroplasmonic properties of the assembled GNRs. A qualitative control of the repulsive force was achieved here by tuning the concentration of CTAB in the as-prepared colloidal solutions, and the relative strength of the repulsive force was estimated by measuring the Zeta-potential (ζ mV, Malvern Zetasizer Nano ZS) of the colloidal systems. Herein the ζ value of discrete GNRs was regulated in the range from ~ 41 to ~ 50 mV. We found that the GNR system showed only slightly different ζ values (see Table S1, ESI†) when changing the solution pH from 7 to 2. This indicates that the CTAB mediated interparticle repulsive force could have nearly the same contribution to the GNR assembly in neutral and acidic environments. As such, we focused on the influence of different chiral interactions on the chiroplasmonic properties of the linear assembly of the GNRs.

CD spectroscopy (Bio-Logic MOS-450) was employed to investigate the chiral interactions during the linear assembly of *L*-, *D*-, and *rac*-GNRs. To characterize the molecular conformations of chiral interactions, the linear chains of *L*-, *D*-, and *rac*-GNRs were encapsulated by negatively charged poly sodium salt (PSS), and then subjected to SERS analyses (Renishaw inVia, 6 mW, 785 nm laser). Furthermore, the dried samples were prepared for the structural characterization by a SEM technique (JOEL JSM-7500F).

Results and discussion

To examine the distinct molecular conformations involved in chiral Zw-Es and Hb interactions, the SERS spectra were

collected from the linear assemblies of L-/D-/rac-GNRs formed in neutral or acidic solutions. Fig. 2a shows the principle Raman bands in the spectral range of 100–1100 cm^{-1} for the linear chains of L-GNRs formed at pH ~ 7 and ~ 3 . The $\sim 180 \text{ cm}^{-1}$ and $\sim 742 \text{ cm}^{-1}$ bands are assigned respectively to the Au–Br and $\text{N}^+(\text{CH}_3)_3$ vibrational modes of the CTAB stabilizers.³⁷ The characteristic SERS signatures of the Cys molecules are recognizable in terms of the previous theoretical and experimental studies^{39,40} (see Table S2 for the assignments of the Cys Raman bands, ESI†). These include the Au–S_{stretching} mode at $\sim 271 \text{ cm}^{-1}$, C–S_{stretching} mode at 662 cm^{-1} , C=O_{deformation} mode at $\sim 495 \text{ cm}^{-1}$, and NCH_{bending} mode at $\sim 973 \text{ cm}^{-1}$. More SERS analyses were conducted for the L-/D-GNR linear assemblies formed in solution with tuned pH values (see Fig. S2–S4, ESI†). We found that the relative intensity of COO vibrations (at $\sim 495 \text{ cm}^{-1}$) with respect to C–S vibrations (at $\sim 662 \text{ cm}^{-1}$), i.e., I_{495}/I_{662} , can be used to distinguish Zw-Es from Hb interactions (Fig. 2a). Moreover, it also allowed us to quantify the transformation between these two interactions in solution. As shown in Fig. 2b, I_{495}/I_{662} displays a minimum value at pH ≥ 6 , a maximum value at pH ≤ 3 , and a steady growth with decrease of the pH in the transition region ($3 < \text{pH} < 6$). This pH-dependent sigmoidal change of the Raman signals reflects the distributions of these two forms of chiral interaction in this pH range:^{33–35} Zw-Es and Hb interactions would exist overwhelmingly in a neutral (pH ≥ 6) or acidic (pH ≤ 3) region,

respectively, while these two forms of interaction could co-exist in the transition region.

For the chiral Zw-Es and Hb interactions with different molecular conformations shown above, the involved chiral information was obtained by CD measurements. Firstly, we examined the optical activity of the discrete L-/D-/rac-GNRs (see Fig. S5, ESI†). The L- and D-GNRs displayed a mirror-image of the CD signals in the UV spectral range (200–350 nm), while the rac-GNRs showed a null CD signal. Given that the same GNRs without Cys patches are intrinsically achiral (see Fig. S5, ESI†), such CD effects were attributed to the chiral active interfaces induced by Cys adsorption.⁴¹ To investigate the chiral Zw-Es and Hb interactions at the interfaces, dynamic CD measurements were conducted during the self-assembly of the L-/D-GNRs. Fig. 2c and d show the time-resolved CD spectra from the assembly of L-GNRs at pH ~ 7 and ~ 3 , respectively (the corresponding extinction spectra can be found in Fig. S6, ESI†). We observed a similar UV-CD feature but dramatically different plasmonic CD responses in the Vis/NIR region. For the case of Zw-Es interactions, the plasmonic CD signal grew steadily with time, and eventually reached a quasi-equilibrium state. In contrast, for the case of Hb interactions, the plasmonic CD signal was almost absent during the whole assembly process. Similar phenomena were observed during the assembly of D-GNRs (see Fig. S7, ESI†). The on/off plasmonic CD signals demonstrate an alternative but clearer way for optically differentiating between the chiral Zw-Es and Hb interactions.

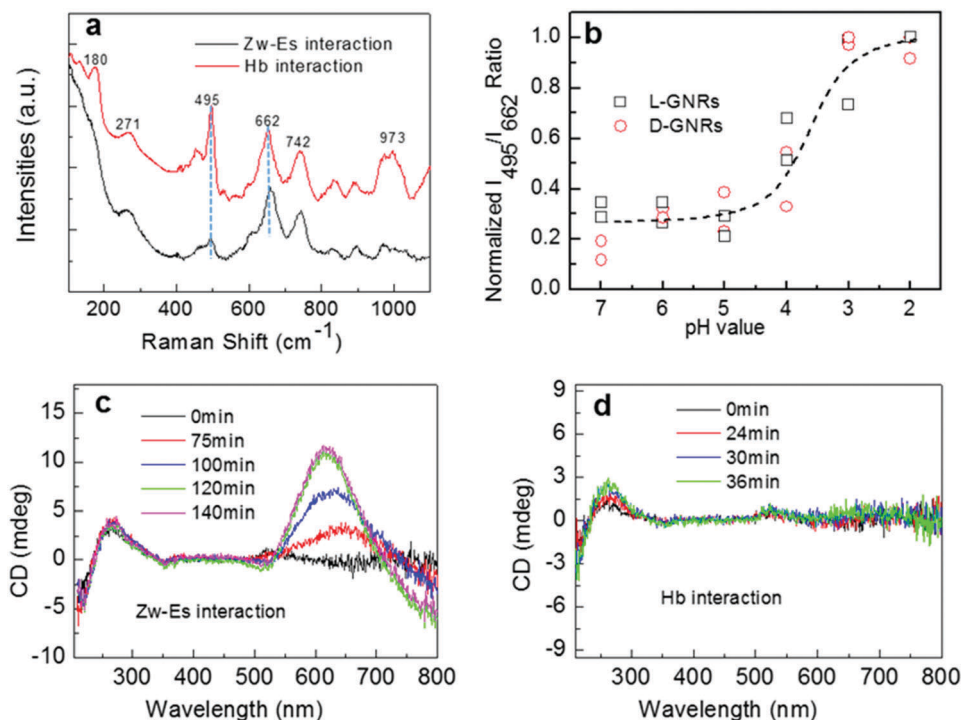


Fig. 2 Raman and CD measurements of GNR based chiroplasmonic nanosensors. (a) SERS spectra of the L-GNR linear assemblies formed via Zw-Es (black line) and Hb (red line) interactions in the range of 100–1100 cm^{-1} . (b) Variation of the intensity ratio, i.e. I_{495}/I_{662} , as a function of the pH values for L-GNR (black squares), and D-GNR (red circles) linear assemblies. The results are shown here for the two independent measurements and the data points were normalized by the maximum value of I_{495}/I_{662} obtained at pH ~ 2 or pH ~ 3 . The dashed line is only for guiding the pH-dependent changes of the I_{495}/I_{662} values. (c and d) The dynamic CD spectra acquired during the assembly process of L-GNRs via Zw-Es (c) and Hb (d) interactions. The assembly time $t = 0$ is referred to as the starting point at which the L-GNR assembly was initiated.

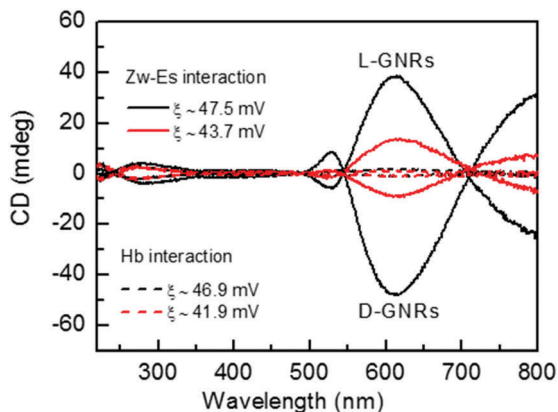


Fig. 3 CD measurements of the chiral Zw-Es (at pH \sim 7, solid lines) and Hb interactions (at pH \sim 3, dashed lines) under the conditions of stronger (larger ζ value) or weaker (smaller ζ value) interparticle repulsive forces. The spectral data were acquired at the quasi-equilibrium stage of L-/D-GNR assembly.

This on/off plasmonic CD effect was also observed from the assembly of L-/D-GNRs with different ζ values in neutral or acidic solutions. As shown in Fig. 3 (also in Fig. S9, ESI †), for the case of Zw-Es interactions, plasmonic CD signals varied with the ζ values, but their spectral profile had an unnoticeable change in the range of ζ discussed here; whereas undetectable plasmonic CD signals appeared invariably for the case of Hb interactions, regardless of a stronger (*i.e.* larger ζ value) or weaker (*i.e.* smaller ζ value) interparticle repulsive force. These results suggest that the repulsive forces have little influence on the plasmonic CD based chiroptical differentiation between Zw-Es and Hb interactions.

For the undetectable plasmonic CD effects in the case of the chiral Hb interactions shown above, we should take great caution regarding the influence of the structures of the L-/D-GNR assemblies. As reported in previous studies,^{24,42} the (partially) disordered structures of L-/D-GNR assemblies can show rather weak and even non-detectable plasmonic CD signals. In this study, the formation of an EE assembly of GNRs was evident by the dynamic extinction spectra (Fig. S6, S7 and S9, ESI †) and SEM images (Fig. S10, ESI †). The former showed the time-dependent growth of coupled plasmon absorptions at longer wavelengths, which are consistent with the previous studies on a Cys mediated EE assembly of GNRs; the latter confirmed a predominant existence of the linear chains. It was also noticed that the L-/D-GNR assemblies formed in both neutral and acidic solutions show a good similarity in their SPR spectra (Fig. S7, ESI †) and linear chains structures (Fig. S10, ESI †). Therefore, the undetectable plasmonic CD effect in acidic solutions is less correlated with the disordered plasmonic structures. Instead, the change of the molecular conformations could have an important influence. As reported very recently by Gang and co-workers,¹⁸ on/off plasmonic CD responses were observed for DNA molecules that are perpendicular/randomly oriented to the Ag nanoparticle surface. Theoretically, such a presence/absence of the plasmonic CD effect could be associated with the different orientations of the molecular electric dipole moments with respect to the axis of the plasmonic structure.⁴³

It is noteworthy that the detectable CD spectral features in the case of the chiral Zw-Es interactions showed strong dependence on the chirality of the Cys patches. As shown in Fig. 3 (also in Fig. S9, ESI †), a nearly mirror-image response was seen in the assembly of L- and D-GNRs, while a null CD activity appeared in the assembly of *rac*-GNRs. These results are evidence of the selectivity of plasmonic CD nanosensors to the interfacial chiral interactions mediated by Cys patches. Furthermore, the ability to discriminate different homochiral (LL and DD) Zw-Es interactions by the opposite signs of the CD signals makes it more advantageous over the chirality-insensitive methods, *e.g.* SPR absorption¹¹ and Raman scattering spectroscopy.^{13,14}

Using penicillamine (Pen), a model drug molecule,⁴⁴ as chiral patches, we further examined the on/off chiroplasmonic responses in the probes of chiral Zw-Es/Hb interactions (see the ESI † for the related Experimental details). Similar to the case of the Cys molecules, L-/D-Pen mediated chiral Zw-Es and Hb interactions led to linear assembly of GNRs in neutral (at pH \sim 7) or acidic (at pH \sim 3) solutions (Fig. S11, ESI †). The different molecular conformations involved in these two interactions were recognizable by SERS spectroscopy. As shown in Fig. 4a (also in Fig. S12, ESI †), two SERS bands (\sim 521 cm^{-1} and \sim 659 cm^{-1}), assigned respectively to the COO_{rocking} and OCO_{bending} modes of Pen molecules,^{45,46} appeared only in the

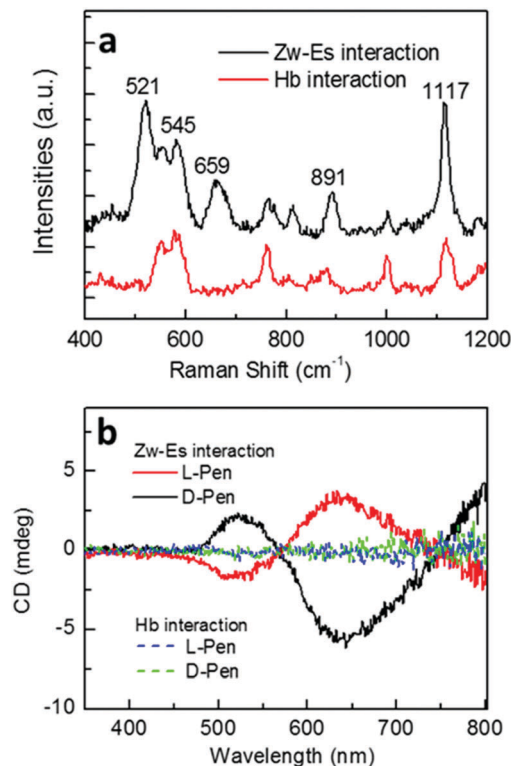


Fig. 4 Detection of Pen mediated Zw-Es and Hb interactions by GNR based chiroplasmonic nanosensors. (a) SERS spectra of L-Pen mediated GNR linear assemblies via Zw-Es (black line) and Hb interactions (red line) in the range of 400–1200 cm^{-1} . (b) CD responses of the GNR linear assemblies for the L-/D-Pen mediated chiral Zw-Es (red and black solid lines) and Hb (blue and green dashed lines) interactions.

case of Zw-Es interactions. Given that Pen patches are protonated in an acidic environment,⁴⁴ it is reasonable that the conformations of the COOH group could be particularly sensitive to the change from Zw-Es to Hb interactions. Fig. 4b shows the plasmonic CD signals acquired from the L-/D-Pen mediated assembly of GNRs in pH ~ 7 and pH ~ 3 solutions. Once again, the plasmonic CD based chiroptical nanosensor allows us not only to differentiate between the chiral Zw-Es and Hb interactions at the interfaces, but also to identify the LL/DD homochiral Zw-Es interactions by a nearly mirror-image of the CD signals.

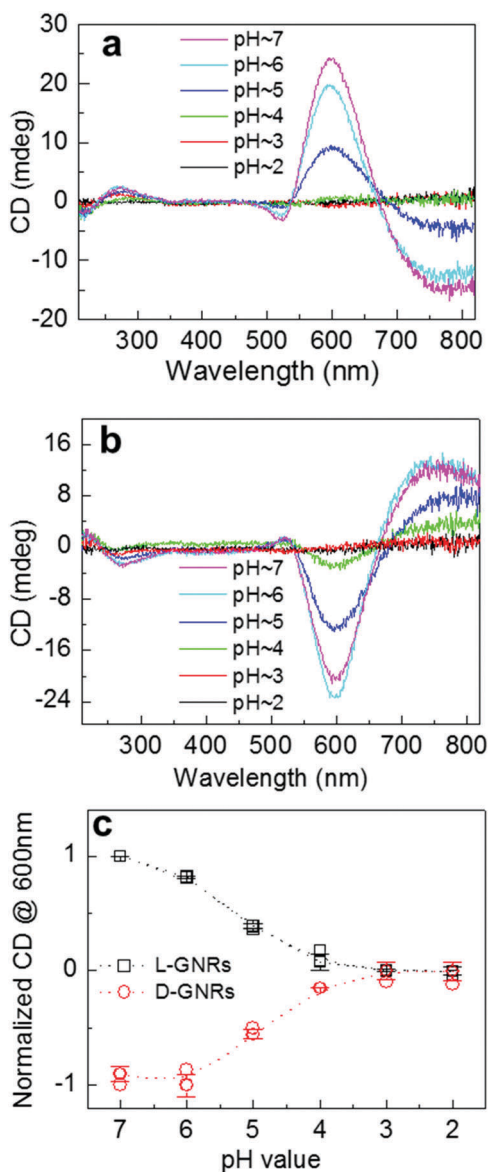


Fig. 5 Selectively probing the chiral Zw-Es interactions in solutions with different pH values. (a and b) pH dependent plasmonic CD spectra from a linear assembly of L- (a) and D- (b) GNRs. (c) Plots of the normalized CD peak-intensities at 600 nm as a function of the pH values for L- (black squares) and D- (red circles) GNR assemblies. The data points were normalized by the maximum value obtained in a neutral environment. The dashed lines are only for guiding the variations of the CD intensity with the change of the pH value.

For both the Cys and Pen molecules, the detectable plasmonic CD signals are specific to the chiral Zw-Es interactions. In light of this specificity, we expected that the plasmonic CD nanosensors can be used to selectively probe the chiral Zw-Es interactions in solution. To verify this, CD analyses were conducted for the assembly of L- and D-GNRs in solution with tuned pH values in the range of 2–7. We found that plasmonic CD intensities did vary with the pH value (see Fig. 5a and b, also Fig. S13 and S14, ESI†). By extracting the peak intensity at 600 nm from each CD measurement, we observed clearly a pH dependent sigmoidal change of the CD strength, as shown in Fig. 5c. In combination with the sigmoidal change of the SERS signals shown in Fig. 2b, the decay of the CD strength with tuning of the pH from 6 to 3 is associated with a reduction of the chiral Zw-Es interactions (or an increase of the chiral Hb interactions) in this transition region. At this point, the plasmonic CD nanosensors can recognize the chiral Zw-Es interactions in solution with different pH values.

Conclusions

In summary, we have revealed that chiroplasmonic nanosensors possess both conformational sensitivity and chiral selectivity to the molecular interactions occurring at nanoscale interfaces in the solution phase. By virtue of this dual function, plasmonic CD nanosensors have been used for in-situ monitoring of the transformation between the chiral Zw-Es and Hb interactions in solution phases, and particularly for recognizing the homochiral Zw-Es interactions in different pH solutions. Nevertheless, future works are still needed for understanding the physical basis that links on/off plasmonic CD responses and the different configurations of the interfacial chiral Zw-Es/Hb interactions. We believe that plasmonic CD based chiroptical nanosensors will open a new pathway for the mechanistic study of biomolecular recognition at nanoscale interfaces in solution phases.

Acknowledgements

W. J. Z. and R. Y. W. gratefully acknowledge the fruitful discussions with Prof. Hongxing Xu from Wuhan University and Prof. Deyin Wu from Xiamen University. This work was supported by the National Natural Science Foundation of China (Grant No. 11574030, 11174033, 11422436, 91127013), and Ministry of Science and Technology of China (Grant No. 2015CB932400 and 2016YFA0200903)

References

- 1 D. B. Amabilino, *Chirality at the Nanoscale: Nanoparticles, Surfaces, Materials and more*, Wiley-VCH Verlag GmbH & Co. KGaA, Weinheim, 2009.
- 2 P. Yin, Z.-M. Zhang, H. Lv, T. Li, F. Haso, L. Hu, B. Zhang, J. Bacsá, Y. Wei, Y. Gao, Y. Hou, Y.-G. Li, C. L. Hill, E.-B. Wang and T. Liu, *Nat. Commun.*, 2015, **6**, 6475.

- 3 J. N. Israelachvili, *Intermolecular and Surface Forces*, Academic Press, London, 3rd edn, 2011.
- 4 K. Ariga, G. J. Richards, S. Ishihara, H. Izawa and J. P. Hill, *Sensors*, 2010, **10**, 6796–6820.
- 5 G. A. Hembury, V. V. Borovkov and Y. Inoue, *Chem. Rev.*, 2008, **108**, 1–73.
- 6 G. Pescitelli, L. Di Bari and N. Berova, *Chem. Soc. Rev.*, 2011, **40**, 4603–4625.
- 7 C. Gautier and T. Bürgi, *J. Phys. Chem. C*, 2010, **114**, 15897.
- 8 K. Osińska, M. Pecul and A. Kudelski, *Chem. Phys. Lett.*, 2010, **496**, 86–90.
- 9 N. Liu, M. Hentschel, T. Weiss, A. P. Alivisatos and H. Giessen, *Science*, 2011, **332**, 1407–1410.
- 10 J. Kumar, A. K. G. Thomas and L. M. Liz-Marzà, *Chem. Commun.*, 2016, **52**, 12555–12569.
- 11 I.-I. S. Lim, D. Mott, M. H. Engelhard, Y. Pan, S. Kamodia, J. Luo, P. N. Njoki, S. Zhou, L. Wang and C. J. Zhong, *Anal. Chem.*, 2009, **81**, 689–698.
- 12 M. Zhang and B. Ye, *Anal. Chem.*, 2011, **83**, 1504–1509.
- 13 W. Liu, Z. Zhu, K. Deng, Z. Li, Y. Zhou, H. Qiu and Y. Gao, *J. Am. Chem. Soc.*, 2013, **135**, 9659–9664.
- 14 Y. Wang, Z. Yu, W. Ji, Y. Tanaka, H. Sui, B. Zhao and Y. Ozaki, *Angew. Chem., Int. Ed. Engl.*, 2014, **53**, 1–6.
- 15 V. K. Valev, J. J. Baumberg, C. Sibilia and T. Verbiest, *Adv. Mater.*, 2013, **25**, 2517–2534.
- 16 A. Ben-Moshe, B. M. Maoz, A. O. Govorov and G. Markovich, *Chem. Soc. Rev.*, 2013, **42**, 7028–7041.
- 17 Z. Zhu, W. Liu, Z. Li, B. Han, Y. Zhou, Y. Gao and Z. Tang, *ACS Nano*, 2012, **6**, 2326–2332.
- 18 F. Lu, Y. Tian, M. Liu, D. Su, H. Zhang, A. O. Govorov and O. Gang, *Nano Lett.*, 2013, **13**, 3145–3151.
- 19 H. Kuang, H. Yin, L. Liu, L. Xu, W. Ma and C. Xu, *ACS Appl. Mater. Interfaces*, 2014, **6**, 364–369.
- 20 W. Ma, H. Kuang, L. Xu, L. Ding, C. Xu, L. Wang and N. a. Kotov, *Nat. Commun.*, 2013, **4**, 2689.
- 21 X. Shen, A. Asenjo-Garcia, Q. Liu, Q. Jiang, F. J. García De Abajo, N. Liu and B. Ding, *Nano Lett.*, 2013, **13**, 2128–2133.
- 22 X. Lan, X. Lu, C. Shen, Y. Ke, W. Ni and Q. Wang, *J. Am. Chem. Soc.*, 2015, **137**, 457–462.
- 23 R.-Y. Wang, P. Wang, Y. Liu, W. Zhao, D. Zhai, X. Hong, Y. Ji, X. Wu, F. Wang, D. Zhang, W. Zhang, R. Liu and X. Zhang, *J. Phys. Chem. C*, 2014, **118**, 9690–9695.
- 24 D. Zhai, P. Wang, R.-Y. Wang, X. Tian, Y. Ji, W. Zhao, L. Wang, H. Wei, X. Wu and X. Zhang, *Nanoscale*, 2015, **7**, 10690–10698.
- 25 S. Hou, H. Zhang, J. Yan, Y. Ji, T. Wen, W. Liu, Z. Hu and X. Wu, *Phys. Chem. Chem. Phys.*, 2015, **17**, 8187–8193.
- 26 Y. Zhao, A. N. Askarpour, L. Sun, J. Shi, X. Li and A. Alù, *Nat. Commun.*, 2017, **8**, 14180.
- 27 J. Slocik, A. Govorov and R. Naik, *Nano Lett.*, 2011, **11**, 701–705.
- 28 H. Zhang and a. O. Govorov, *Phys. Rev. B: Condens. Matter Mater. Phys.*, 2013, **87**, 1–8.
- 29 W. Zhang, T. Wu, R. Wang and X. Zhang, *J. Phys. Chem. C*, 2017, **121**, 666–675.
- 30 M. L. Nesterov, X. Yin, M. Schäferling, H. Giessen and T. Weiss, *ACS Photonics*, 2016, **3**, 578–583.
- 31 P. K. Sudeep, S. T. S. Joseph and K. G. Thomas, *J. Am. Chem. Soc.*, 2005, **127**, 6516–6517.
- 32 G. Gonella, S. Terreni, D. Cvetko, A. Cossaro, L. Mattera, O. Cavalleri, R. Rolandi, A. Morgante, L. Floreano and M. Canepa, *J. Phys. Chem. B*, 2005, **109**, 18003–18009.
- 33 W. Ni, R. a. Mosquera, J. Pérez-Juste and L. M. Liz-Marzán, *J. Phys. Chem. Lett.*, 2010, **1**, 1181–1185.
- 34 A. Filimon, P. Jacob, R. Hergenröder and A. Jürgensen, *Langmuir*, 2012, **28**, 8692–8699.
- 35 R. G. Acres, V. Feyer, N. Tsud, E. Carlino and K. C. Prince, *J. Phys. Chem. C*, 2014, **118**, 10481–10487.
- 36 S. Garten, P. U. Biedermann, S. Topiol and I. Agranat, *Chirality*, 2010, **22**, 662–674.
- 37 S. Lee, L. Anderson, C. Payne and J. Hafner, *Langmuir*, 2011, **27**, 14748–14756.
- 38 K. J. M. Bishop, C. E. Wilmer, S. Soh and B. a. Grzybowski, *Small*, 2009, **5**, 1600–1630.
- 39 E. Podstawka, Y. Ozaki and L. M. Proniewicz, *Appl. Spectrosc.*, 2005, **59**, 1516–1526.
- 40 G. D. Fleming, J. J. Finnerty, M. Campos-Vallette, F. Celis, A. E. Aliaga, C. Fredes and R. Koch, *J. Raman Spectrosc.*, 2009, **40**, 632–638.
- 41 T. Bürgi, *Nanoscale*, 2015, **7**, 15553–15567.
- 42 B. Han, Z. Zhu, Z. Li, W. Zhang and Z. Tang, *J. Am. Chem. Soc.*, 2014, **136**, 16104–16107.
- 43 W. Zhang, T. Wu, R. Wang and X. Zhang, *Nanoscale*, 2017, **9**, 5110–5118.
- 44 C. Chiu, *Anal. Profiles Drug Subst.*, 1981, **10**, 601–637.
- 45 P. Taladriz-Blanco, N. J. Buurma, L. Rodríguez-Lorenzo, J. Pérez-Juste, L. M. Liz-Marzán and P. Hervés, *J. Mater. Chem.*, 2011, **21**, 16880–16887.
- 46 M. R. López-Ramírez, J. F. Arenas, J. C. Otero and J. L. Castro, *J. Raman Spectrosc.*, 2004, **35**, 390–394.